Tidal-stream energy resource characterisation for the Gulf of California, México

Mejia-Olivares, Carlos; Haigh, I.D.; Wells, Neil; Coles, Daniel; Lewis, Matthew; Neill, Simon

Energy

DOI:
10.1016/j.energy.2018.04.074

Published: 01/08/2018

Peer reviewed version

Accepted Manuscript

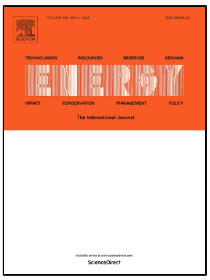

Tidal-stream energy resource characterisation for the Gulf of California, México

Carlos Joel Mejia-Olivares, Ivan D. Haigh, Neil C. Wells, Daniel S. Coles, Matt J. Lewis, Simon P. Neill

PII:	S0360-5442(18)30681-9
DOI:	10.1016/j.energy.2018.04.074
Reference:	EGY 12713
To appear in:	*Energy*
Received Date:	11 December 2017
Revised Date:	16 March 2018
Accepted Date:	13 April 2018

Please cite this article as: Carlos Joel Mejia-Olivares, Ivan D. Haigh, Neil C. Wells, Daniel S. Coles, Matt J. Lewis, Simon P. Neill, Tidal-stream energy resource characterisation for the Gulf of California, México, *Energy* (2018), doi: 10.1016/j.energy.2018.04.074

Tidal-stream energy resource characterisation for the Gulf of California, México

Carlos Joel Mejia-Olivares[1], Ivan D. Haigh[1], Neil C. Wells[1], Daniel S. Coles[2], Matt J. Lewis[3] and Simon P. Neill[3]

[1] Ocean and Earth Science, National Oceanography Centre, University of Southampton, European Way, Southampton, SO14 3ZH, U.K.

[2]Energy and Climate Change Division, Sustainable Energy Research Group, Faculty of Engineering and the Environment, University of Southampton, UK

[3]School of Ocean Sciences, Bangor University, LL59 5AB, UK.

Corresponding author

E-mail address: carlos.mejia-olivares@noc.soton.ac.uk (Carlos Joel Mejia-Olivares).
Ocean and Earth Science, National Oceanography Centre, University of Southampton, European Way, Southampton, SO14 3ZH, U.K.

Submit to Energy

December 2017

Abstract

There has been a growing interest in tidal-stream energy, with most past studies focusing on assessing the potential resource of sites with fast tidal currents in relatively shallow water. Regions with less energetic tidal currents, but in deeper waters, have been overlooked. One potential tidal-stream energy region, which fits this categorization, is the Gulf of California. In this paper we quantify the theoretical tidal-stream energy resource in this region. The resource is estimated with an unstructured depth-averaged hydrodynamic model. We find that the highest flow speeds of 2.4 m/s occur in the channel between San Lorenzo and San Esteban Island, and three lower-velocity potential sites are identified in the channels between: (1) Baja California Peninsula and San Lorenzo Island; (2) San Esteban and Tiburon Islands and (3) Baja California Peninsula and Angel de la Guarda Island. Although peak kinetic power density in these regions is found to be relatively low (~ 3 to 6 kW/m^2), the large water depth (100 to 500 m), results in an undisturbed theoretical annual mean power of between 100 to 200 MW. We therefore find the tidal energy resource to be large, but new turbine technologies would be required to exploit these 'next generation' resource regions.

Key words: tidal-stream energy; kinetic power density; mean annual power; Gulf of California; México

Highlights

- Barotropic model predicted peak tidal flows between 1.0 and 2.4 m/s at sites in the Gulf of California;
- Theoretical tidal-stream power density estimates at four sites were ~ 3 to 6 kW/m^2;
- Resource could be high as potential sites in deep water (100 to 500 m) but new technologies required for these non-traditional regions.

1. Introduction

Over the last two decades there has been increased interest in tidal stream energy exploitation [1]. Tidal energy resource offers many benefits compared to other sources of renewable energy, because of the regular and predictable nature of ocean tides. The annual theoretical power of the tidal-stream resource world-wide has been estimated to be in the order of 10×10^4 TWh [2]. However, in practice only a limited percentage of that energy can be converted into electrical energy due to technical and practical constraints [1,3,4]. As interest in tidal-stream energy increases, detailed tidal energy resource assessments have now been undertaken for many regions, including sites in the: UK [5,6,7,8]; Canada [9,10,11]; France [12,13,14; Norway [15]; Spain [16,17]; Indonesia [18,19]; Taiwan [20], China [21]; Malaysia [22]; Philippines [23]; and New Zealand [24,25].

In recent years, there has been growing interest in exploiting tidal stream energy extraction for countries within Latin America. In the developing countries in Latin America, in particular, the demand for electricity has increased considerably in recent decades due to economic development [26]. Osorio et al. [27] undertook a tidal-stream energy assessment for Buenaventura Bay in Colombia, and estimated that the kinetic power density (KPD) for that region was relatively small, in the order of 0.04 kW/m^2, with the maximum current speed being 0.7 m/s. Herrera et al. [28] suggested that there might be locations in Strait of Magellan in southern Chile that may be feasible for tidal-stream energy extraction, with an estimated mean KPD exceeding 10 kW/m^2. González-Gorbeña et al. [29] carried out a tidal-stream energy assessment for San Marcos Bay in Brazil and estimate the resource to be between 9.2 and 11.2 MWh/m^2. Another assessment undertaken in the same country by Marta-Almeida et al. [30] indicated that the potential KPD available at Baiá de Todos os Santos is between 1.3 and 2.5 kW/m^2, with maximum peak tidal flow velocities of 1 m/s. Alonso et al. [31] assessed the potential tidal-stream energy resource between La Paloma and Cabo Polonio on the Atlantic coast of Uruguay, and estimated a KPD of 0.06 kW/m^2.

México has set an ambitious target of supplying 35% of its total energy from renewable sources by 2027 [32]. Also in 2015, the Mexican government agreed, through the United Nations, to reduce 22% of its fossil fuels use by 2030 [33]. Currently 19% of México's electricity is produced through renewable sources, which mainly comprises solar, wind and hydropower sources [26]. In 2009, Hiriart-Le Bert and Silva-Casarin [34] assessed the feasibility and

potential energy resource for a tidal barrage situated in the northern most reaches of the Gulf of California. They estimated the annual electricity production to be in the range of 872 to 17,325 (GWh). Tapia et al. [35] estimate tidal-range power for three specific sites in the Gulf of California: San Rafael Bay (14 MW); Bay of Soldado (1.3 MW); Bay of Santa Maria (2.5 MW). However, to date, no detailed assessment of the tidal-steam energy resource has been produced for Mexico, despite the fact that peak spring tidal flows of over 1.5 m/s have been measured between the Midriff Islands in the Gulf of California (GC) [36,37] (Fig. 1). Therefore, this region holds promise for tidal-stream energy extraction, and hence is the focus of this study. In contrast to other regions in which the tidal stream energy resource has been explored, the GC is relatively deep, and diurnal tidal constituents are typically larger; hence the resource characterization is expected to contrast considerably from previously identified tidal stream sites. Therefore, the aim of this paper to is to address that gap by undertaking a detailed quantification of the tidal-stream energy resource in the GC.

The GC, also known as the Sea of Cortez, is a semi-enclosed sea (Fig. 1a). Its length is about 1,100 km and its width varies between 48 and 240 km. It covers an area of 177,000 km^2. The GC has a complex bathymetry and encompasses over 800 islands. Its depth varies from around an average depth of 200 m in the upper Gulf to 3,600 m at its entrance with the Pacific Ocean. The Midriff region contains several larger islands (e.g. Smith, Salsipuedes, San Lorenzo and San Esteban Island), and the two biggest in the Gulf, namely, Angel de la Guarda Island and Tiburon Island (Fig. 1b). These Islands form channels in this region. The area of most interest to this study is the region around the Midriff Islands (Fig 1b), as results from a previous study indicates that tidal currents here exceed 1.5 m/s [36,37].

The GC has areas of high tides, strong tidal mixing, stratification, internal waves and a unique combination of warm temperatures and high nutrient concentrations, making the area extremely biodiverse [38,39]. The tides in the GC are produced by co-oscillation between the GC and the Pacific Ocean [40,41]. A detailed study of tides in the region has been carried out by Marinone [42]. Tides are semi-diurnal in the northern and southern part of the GC and are diurnal in the central region to the south of the Midriff region. Due to resonance, the tidal range is largest in the northern most region. The dominant tidal constituents are the M_2, S_2, K_1, and O_1. M_2 amplitude increases from 0.36 m at the mouth of the Gulf to 1.5 m at the northern most region. This amplification occurs as a consequence of the resonant response of those frequencies in the GC.

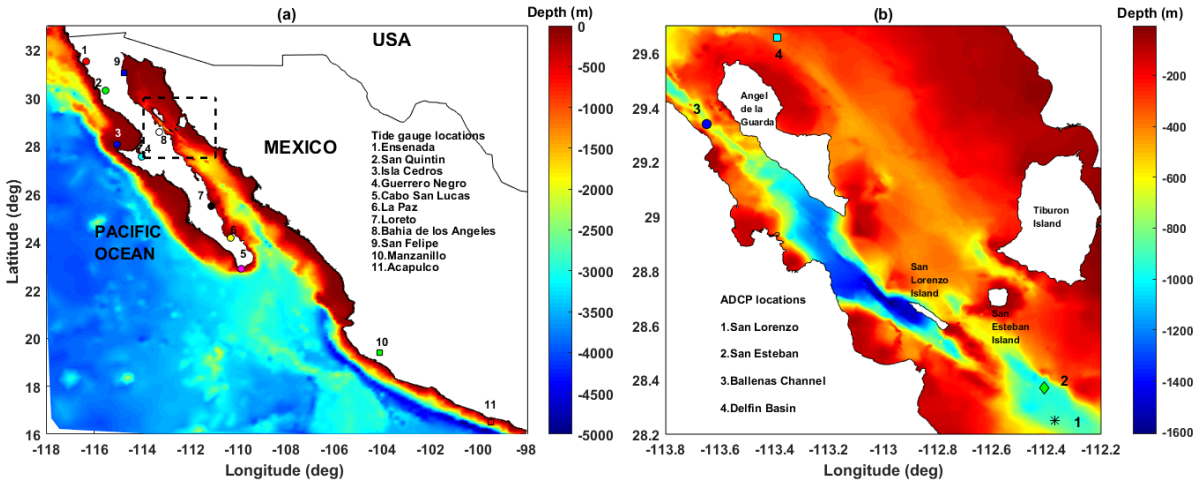

Figure 1: Location of the study area with water depths for the: (a) Gulf of California, with the locations of the tide gauge sites; and (b) the Midriff region, with the locations of the ADCP sites.

The structure of the paper is as follows: In Section 2 we describe the numeral model we have setup for the region. In particular, we describe how we have configured the unstructured depth-averaged hydrodynamic model of the the Gulf of California using the TELEMAC suite of modelling tools (Section 2.1). We then discuss how we have validated the model against water levels and velocity measurement, including detailed validation statistics (Section 2.2). In Section 3 we then describe how we have used the model results to assess current speeds and estimate the energy resources of the region. In particular, we describe how we determined the location of the fastest currents, their magnitude and how we compare the flows vary over a tidal cycle and a spring/neap period (Section 3.1). We detail how we quantify the theoretical, undisturbed tidal-stream energy resource across the region (Section 3.2). Finally, we describe a series of sensitivity tests we undertook to determine the influence of using different bathymetry products (Section 3.3). In Section 4 we describe the results. First, we discuss the analysis of currents speeds (Section 4.1); second, we describe the energy resource assessment (Section 4.2); and third, we detail the results of the sensitivity tests in which we have run simulations with varying bathymetries (Section 4.3). Key findings are discussed in Section 5 and conclusions are given in Section 6.

2. Gulf of California model configuration and validation

2.1 Model configuration and domain

A depth-averaged barotropic model was configured using the TELEMAC modelling suite of tools, covering the Mexican Pacific coastal region and the GC (Fig. 2). The TELEMAC modelling system was chosen for its computing performance, the fact it is open source and for its finite element method, which enables variable mesh resolution to focus modelling effort in areas of interest [43]. Its 2D component, TELEMAC-2D, is based on the numerical solutions of the shallow water equations, or St Venant equations. It solves the vertically integrated equations of momentum balance and the continuity equations. The shallow water equations are applicable where there is a scale relationship between the horizontal and vertical length scale and where the vertical velocities can be considered negligible and the pressure treated as hydrostatic. This assumption along with depth integration reduces the Navier-Stoke equations to incompressible flow. TELEMAC is a popular model choice for tidal energy resource assessment and characterization [e.g. 5,11,13].

The model mesh was generated using the Blue Kenue software and is shown in Fig. 2. The mesh consists of 38,181 nodes and 133,779 elements. It has a resolution of 0.507° (~60 km) at the open boundary condition in the Pacific and increases to 0.042° (~5 km) at the entrance to the GC (Fig. 2a). Within the GC the resolution increases to 0.0083° (~1 km) around the Midriff Islands (Fig. 2b) and reduces to 0.025° (~3 km) resolution at the northern most reaches.

The primary bathymetry data interpolated onto the model mesh was from the General Bathymetry Chart of the Oceans (GEBCO dataset) [44] at 30 arc-second resolution (~900 m). In addition, higher resolution (~450 m) bathymetry data in northern GC, was merged within the GEBCO gridded data. This dataset was obtained from The Center for Scientific Research and Higher Education at Ensenada (CICESE). The inclusion of the higher-resolution bathymetry data in the northern GC significantly improved the tidal level and current validation, compared to using just the GEBCO bathymetry alone, as we will discuss later.

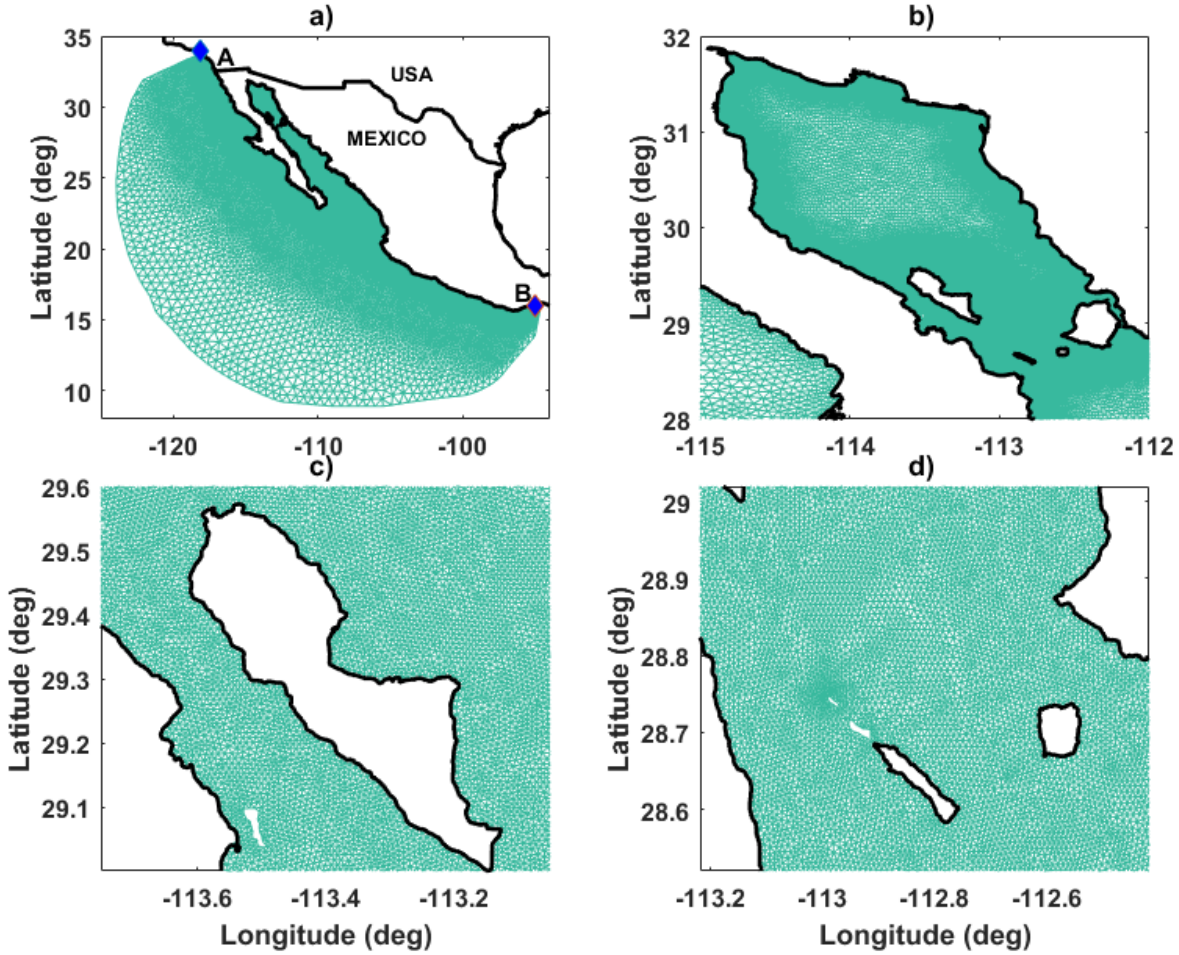

Figure 2: Model mesh cover the (a) Gulf of California Full mesh of the model and boundary conditions points, zoomed into the Northern and central GC (b) and zoom into Midriff region (c) and (d)

The open ocean boundaries (located between points A and B, shown in Fig 2a) were driven using tidal levels predicted from the TPXO 7.2 dataset [45,46]. TPXO is derived from OTIS (Oregon State University Tidal Inversion Software), which assimilates data from the TOPEX/Poseidon and Jason altimetry missions. This global model provides amplitudes and phases for the eight main diurnal and semi-diurnal constituents (M_2, S_2, N_2, K_1, O_1, P_1, Q_1), three non-linear constituents (M_4, MS_4, MN_4), and two long period constituents (Mf, Mm), at 1/4 degree resolution. The harmonic constituents were obtained from the OTIS Website (http://volkov.oce.orst.edu/tides/global.html) and subsequently the tide was predicted using the Tidal Model Driver (TMD) Matlab routines that include the 4.4-year perigean cycle and the 18.6-year lunar nodal cycle [47].

2.2 Model Validation

The model was validated against water levels measured from tide gauges and u and v current velocities measured by acoustic Doppler current profilers (ADCP). These datasets were obtained from CICESE. Data for 11 tide gauge stations were used [48], the locations/details of which are listed in Table 1 and shown in Fig. 1a. Current measurements were also obtained from CICESE at 4 sites around the Midriff Islands in the GC, the locations of which are listed in Table 2 and shown in Fig. 1b. These ADCP current measurements were available every hour through the water column and were collected using a 150 kHz ADCP deployed 8 and 7 m above the seabed and the bin depth was 10 m [37].

Table 1: Details of the tide gauge records used for model validation

Site Number	Site Name	Reference Code	Longitude (decimal degree)	Latitude (decimal degree)	Period	Number of months (range)
1	Ensenada	ENSM	-116.38	31.52	From January to December 2015	12
2	San Quintin	SNQN	-115.59	30.29		
3	Isla Cedros	ICDN	-115.11	28.05		
4	Guerrero Negro	GROM	-114.09	27.53		
5	Cabo San Lucas	CSLN	-109.54	22.52	From 24 of November to 31 of December 2015	1.5
6	La Paz	LPAZ	-110.35	24.16	From January to December 2015	12
7	Loreto	LTON	-111.80	25.48	23 of November to 31st of December 2015	1.5
8	Bahia de los Angeles	BLAN	-113.33	28.57	From January 2015 to December except June and July 2015	10

9	San Felipe	SNFN	-114.82	31.02	From January to December 2015	12
10	Manzanillo	MNZN	-104.17	19.38	From January to December 2015	12
11	Acapulco	ACAN	-99.55	16.5	24 of September to 31st of December 2015	1.5

Table 2: ADCP data records used for current validation

Reference Code	Site Name	Longitude (decimal degree)	Latitude (decimal degree)	Period	Number of months - period
SL	San Lorenzo	-112.37	28.25	From May 2003 and November 2004	18
SE	San Esteban	-112.41	28.37	From May 2003 and November 2004	18
BC	Ballenas Channel	-113.65	29.34	From May 2003 and November 2004	18
DEL	Delfin	-113.39	29.655	September 2005 to September 2006	18

A harmonic analysis of the tide gauge records was undertaken using the T-Tide software to extract just the astronomical tidal component [49]. The depth averaged currents at each of the four ADCP site were also calculated. Again, a harmonic analysis was undertaken on the observed u and v velocity components, to extract just the astronomically driven tidal components. For validation, the model was run for the period from 27 November 2015 to 31 December 2015, and results were saved at every grid point every 10 minutes. The first three days were considered as model spin up and were not included in the subsequent analysis.

Different statistical methods were used to assess the performance of the hydrodynamic model in reproducing tidal levels and tidal currents at each observational site. To determine how accurately the model predicts both the tidal levels and currents in the region, the amplitude and

phase of the main tidal constituents, extracted from both the measured and predicted water levels using T-Tide, were compared. In addition, three error measures were used to quantify the model skill. For each of the time-series, the absolute difference between each 10-minute measured and predicted value was computed. The mean, equivalent to root mean square error (RMSE), and standard deviation of the absolute differences were calculated. The percentage error was derived by dividing the RMSE by the tidal range or range of the tidal current magnitudes. Correlation coefficients between the measured and predicted time-series were also derived for each complete time-series.

A comparison of the amplitude and phase of the four main tidal level constituents (M_2, S_2, K_1 and O_1) across the 11 tide gauge sites is shown in Fig. 3, for the measured and modelled time-series. The results show good agreement for each of the main tidal constituents. The model predictions capture the range of amplitudes across the study area. The mean absolute error between the amplitude and phase for the main tidal constituents, across the 11 sites, are listed in Table 3. The mean amplitude differences are less than 7 cm for the main constituents, with the exception of K_1. The mean phase differences are 10° or less for M_2 and O_1, while the remaining constituents are less than 21° different.

A comparison of the measured and predicted tidal level time-series at a selection of the tide gauge sites are shown in Fig. 4. The model predictions again show good agreement with measurements across the model domain. The model accurately captures the variation in both the tidal range and tidal form (i.e. semi-diurnal and mixed) across the study domain, and for both spring and neap periods.

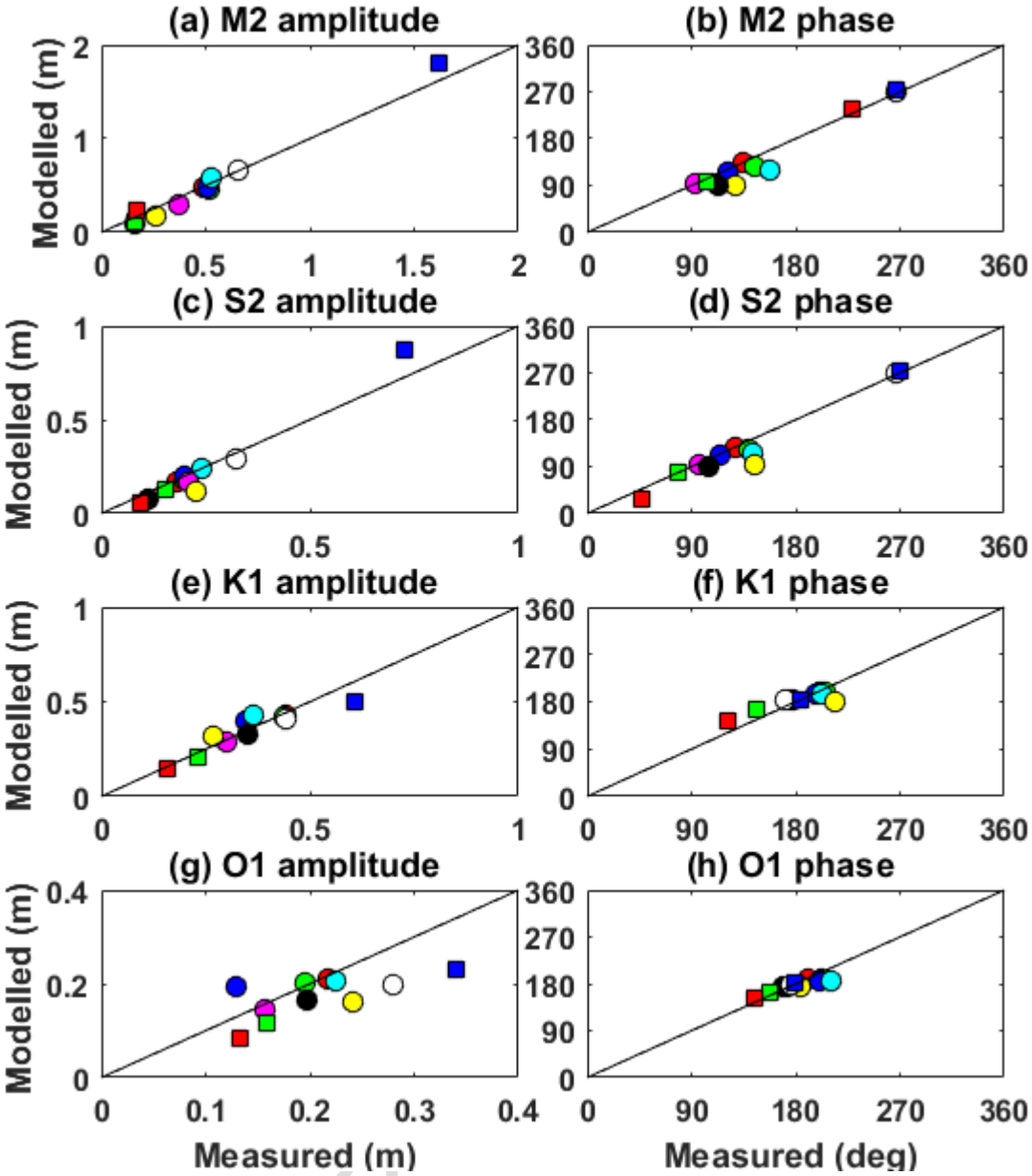

Figure 3: Comparison of the measured and predicted amplitudes and phases of the four main tidal constituents for the 11 tide gauge sites.

Table 3: Mean absolute differences between the measured data and TPOX7.2 global ocean tidal model for the 11 Validation sites.

Tidal constituent	Mean absolute error of the amplitude (m)	Mean absolute error of phase (degrees)
M_2	0.07	10
S_2	0.04	19
N_2	0.02	13
K_1	0.20	21
O_1	0.05	9
Q_1	0.00	20

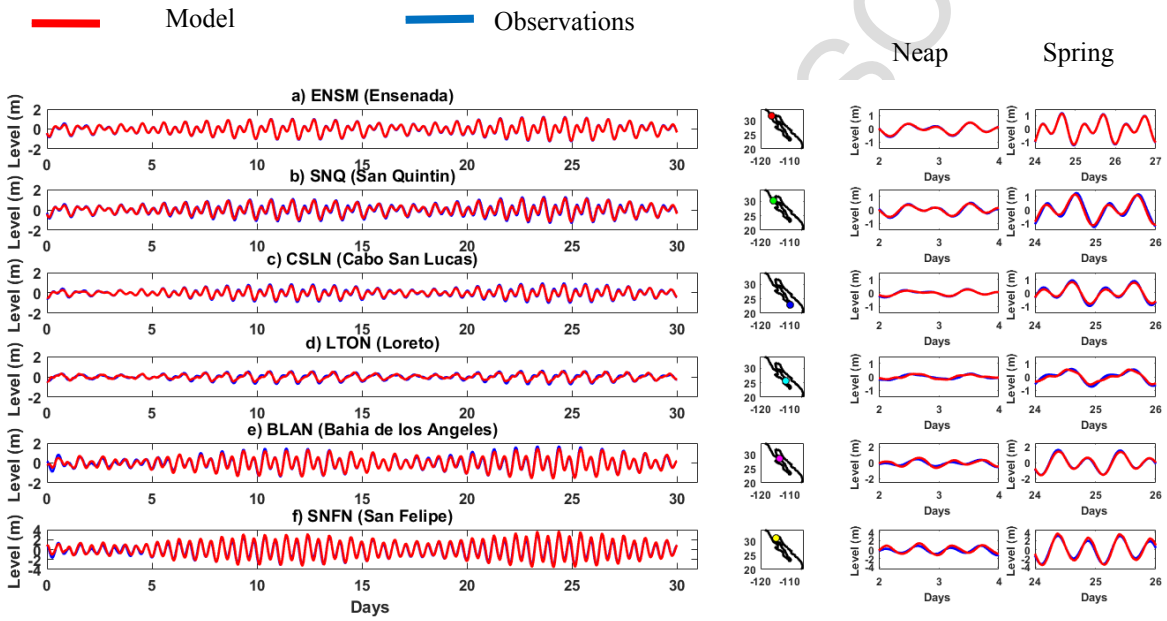

Figure 4: Comparison of the measured and predicted tidal time-series at selected tide gauge sites.

Four error measures were used to quantify the model skill at the 11 tide gauge sites, and these are listed in Table 4. The largest RMSE is at Guerrero Negro (0.26 m) while the smallest are at Ensenada (0.03 m), Cabo san Lucas (0.06 m) and Loreto and Manzanillo (0.07 m). The mean of RMSE across all sites is 0.11 m. The percentage errors are largest at La Paz (11%) but are less than 10% are the reminding 10 tide gauge sites. The larger error at La Paz could be a result of the fact that the tide gauge is in an enclosed bay with a complex bathymetry that is not accurately represented at our current model resolution (3 km in this region). The mean standard deviation error across the validation sites is 0.08 m and the mean correlation coefficient is 0.94. In conclusion, the model does a good job of reproducing tidal levels across the region.

Table 4: Statistic error measures for the 11 tide gauges stations

Site number	Site Name	RMSE (m)	% Error	STD (m)	Correlation Coefficient
1	Ensenada	0.03	1.2	0.02	0.99
2	San Quintin	0.11	4.5	0.07	0.97
3	Isla Cedros	0.10	4.4	0.09	0.96
4	Guerrero Negro	0.26	9.6	0.15	0.84
5	Cabo San Lucas	0.06	3.0	0.04	0.99
6	La Paz	0.19	10.9	0.12	0.75
7	Loreto	0.08	5.9	0.05	0.95
8	Bahia de los Angeles	0.09	3.0	0.07	0.98
9	San Felipe	0.25	3.8	0.17	0.99
10	Manzanillo	0.07	6.1	0.05	0.94
11	Acapulco	0.07	7.7	0.05	0.91
All	**Mean**	**0.11**	**5.0**	**0.07**	**0.86**

A comparison of the depth-averaged amplitude and phase of the u and v tidal velocities components (estimated from the measured and predicted datasets at each of the validation sites) are shown in Fig. 5 and Fig. 6, respectively, for the four ADCP sites. There is reasonable agreement between the model predictions and the observational data. For the M_2 tidal current constituent, mean absolute errors across the four sites for the u and v components are below 0.01 m/s (Table 5). For S_2, the mean absolute error in the u amplitude is 0.01 m/s and is 0.19 m/s in the v component. The mean absolute phase error for M_2 and S_2 is less than 2 degrees for both velocities components. The biggest phase errors were for the K_1 tidal constituents and these were 28 and 30 degrees for the u and v velocity components, respectively (Table. 5). A comparison of the measured and predicted u and v time-series velocities showed (results not shown) good agreement at Ballenas channel (BC) and Delfin Basin (DEL), but currents speeds were underestimated at San Esteban (SE) and San Lorenzo (SL). The latter two sites lie in areas not covered by the high-resolution bathymetry data and this maybe the reason poorer agreement is obtained.

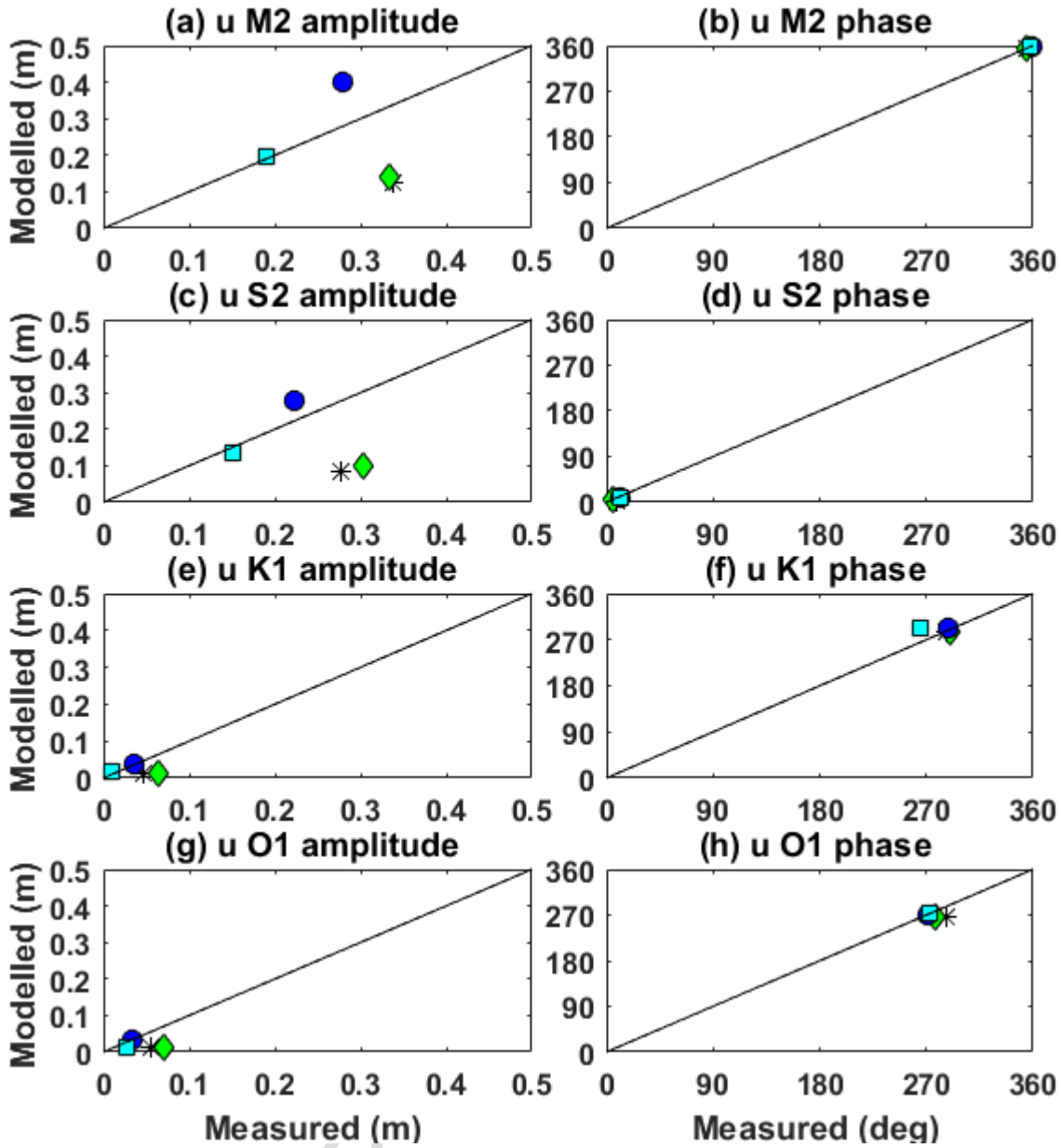

Figure 5: Comparison of the measured and predicted u velocity amplitudes and phases at the four ADCP sites for the: (a) M_2 amplitude; (b) M_2 phase; (c) S_2 amplitude; (d) S_2 phase; (e) K_1 amplitude; (f) K_1 phase; (g) O_1 amplitude; and (h) O_2 phase.

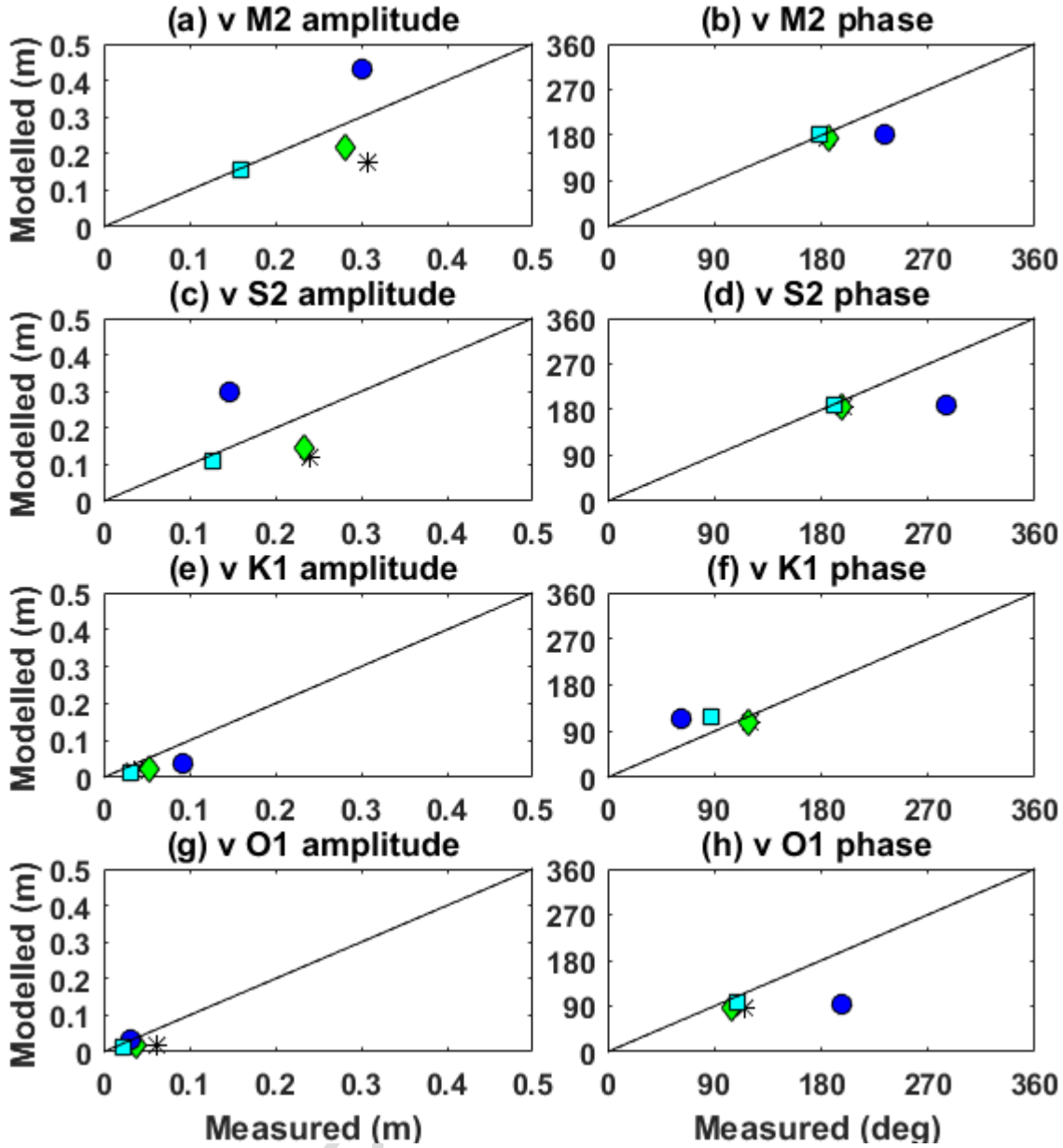

Figure 6 : Comparison of the measured and predicted v velocity amplitudes and phases at the four ADCP sites for the: (a) M_2 amplitude; (b) M_2 phase; (c) S_2 amplitude; (d) S_2 phase; (e) K_1 amplitude; (f) K_1 phase; (g) O_1 amplitude; and (h) O_2 phase.

Table 5: Mean absolute amplitude and phase from the main tidal constituents, estimated data and measured ADCP and tidal constituents across all sites

Tidal constituent	Mean absolute error of the amplitude u velocity component (m/s)	Mean absolute error of the amplitude v velocity component (m/s)	Mean absolute error of phase (degrees) u velocity component	Mean absolute error of phase (degrees) v velocity component
M_2	0.01	0.00	1	1
S_2	0.01	0.19	1	0

N_2	0.01	0.02	5	3
K_1	0.01	0.01	28	30
O_1	0.01	0.10	0	12
Q_1	0.00	0.00	21	12
All Mean	**0.01**	**0.05**	**9**	**10**

Similarly, four error measures were used to quantify the model skill at the four ADCP sites, and these are listed in Table 6. The largest RMSE of the u velocity component is at San Esteban (0.19 m/s) and San Lorenzo and (0.18 m/s), while the smallest errors are at Delfin Basin (0.02 m/s) and Ballenas Channel (0.09 m/s). This equates to a percentage error of less than a 7% error at Delfin Basin and Ballenas Channel, but 11% error at San Esteban and San Lorenzo. As mentioned previously, the latter two sites lie in areas not covered by the high-resolution bathymetry data and this maybe the reason poorer agreement is obtained. RMSE and percentage errs in the v component are smaller than in the u component at San Lorenzo, San Esteban and Delfin, but are larger at Bellenas Channel (0.32 m, 25%). The mean standard deviation across the four validation sites is 0.06 m/s and 0.08 m/s for the u and v velocities components, respectively. The mean correlation coefficient is 0.79 and 0.64 for u and v components respectively. In general, these results demonstrate that the model performs reasonably well in reproducing the tidal currents in the Midriff area, particularly in areas where we have access to higher resolution bathymetry data.

Table 6: Root mean square error of u and v velocity components

Site Name	**RMSE(m/s)**		**% Error u**	**% Error v**	**STD (m/s)**		**Correlation Coefficient**	
	u	v	u	v	u	v	u	**v**
San Lorenzo	0.18	0.12	11.3	8.5	0.13	0.08	0.99	0.97
San Esteban	0.19	0.10	11.5	6.7	0.13	0.07	0.97	0.94
Ballenas Channel	0.09	0.32	6.7	25.0	0.06	0.23	0.99	0.34
Delfin	0.02	0.03	2.7	3.7	0.02	0.02	0.99	0.98
Mean	**0.12**	**0.14**	**6.4**	**8.8**	**0.06**	**0.08**	**0.79**	**0.64**

3.0 Methodology for resource characterization

In this Section, we describe how we have used the validated model to assess current speeds and estimate the energy resources of the region, including undertaking sensitivity tests using different bathymetry sources in the model.

3.1 Tidal currents analysis

Once the model was validated we assessed current speeds across the GC, with a focus on the Midriff region, to determine the location of the fastest currents, their magnitude and how the flows vary over a tidal cycle and a spring/neap period. To do this we simulated tidal currents for a 30-day period in March 2015, when tidal currents are expected to be largest due to the large equinox tides that occur around that time each year. Results were saved for each grid point every 10 minutes. Predicted u and v current velocities components were converted into speed and direction.

Current vector plots were produced over a single tidal cycle to examine the characteristics of tidal currents in the region. The maximum current speed was calculated for each grid point for the full 30-day period. Then maximum spring and neap, and ebb and flood current speeds were also calculated. The maximum neap velocity was calculated for the period from the 12-16 March 2015, and the maximum spring velocity was calculated for the period from the 19-23 March 2015. The maximum currents speed values in the ebb and flood period occurred around the 22 March 2015. Note, in this analysis our focus is on depth-averaged currents.

3.2 Methodology to assess the kinetic energy resource

Next, we quantified the theoretical, undisturbed tidal-stream energy resource of the GC, with a focus on the Midriff region because the highest current speeds are observed here. The tidal stream energy resource was calculated using the tidal current harmonics from the simulated current speeds over the 30-day simulation period in March 2015. To avoid computational constraints, we used the tidal current harmonics to predict the tidal currents for a full year, to obtain mean annual values of velocity and kinetic power density, again using the T-Tide software [49]. The instantaneous undisturbed 'theoretical' KPD (per unit area) was calculated as [3]:

$$P_{KPD} = \frac{1}{2}\rho V^3 \quad [4]$$

Where P_{KPD} is the instantaneous undisturbed theoretical Power density in kw/m^2, ρ is water density (1020 kg/m^3) and V is the depth-averaged current velocity (m/s). Turbine power output depends on the cube of current speed, highlighting the importance of high current speeds to tidal-stream energy resource. The KPD is defined as the average quantity of power per unit area available across a surface. In the case of marine current turbines, the cross-sectional area refers to the diameter or the swept area that is in direct contact with the incoming flow. Here, the theoretical KPD was calculated assuming no device interaction with the resource and assuming a one square meter cross-sectional area.

Then we undertook a second analysis to estimate the maximum instantaneous undisturbed 'theoretical' power (P) in Watts [50] as follows:

$$P = \frac{1}{2}\rho A V^3 \quad [5]$$

Where ρ is water density (1020 kg/m^3), V is the depth-averaged current velocity (m/s) and A is the swept area of a tidal turbine (m^2). The instantaneous power represents the kinetic power density multiplied by the swept area (down through the water column). We interpolated current speeds from our flexible mesh onto a regular mesh, with a resolution of 5 km. As a first order approximation, we calculated A as being the water depth of each cell multiplied by the width of the cell (i.e. 5,000 m). Although devices capable of a swept area in the order of 100 - 500 m (the typical water depths in our study area) are not currently being developed, this approach provides an estimate of the maximum theoretical resource available. We stress than this is a significant over-estimation of the available resource, as it would not be possible to utilize the full water column at 100% efficiency. Never-the-less it provides a useful first approximation to inform industry and policy and demonstrate, as we will stress later, that sites with slower tidal current speeds, but lower water, have a potentially large tidal stream energy resource. Also, in the future, the innovative development of emergence of tethered floating devices (i.e. 3rd/4th/5th/ generation tidal-stream devices) will be able to utilise this theoretical resource in greater water depths.

3.3 Influence of bathymetry

In Section 2, we described how the model validation improved when we merged higher resolution bathymetry data for the Midriff region (obtained from CICESE with a resolution of ~450 m) within the GEBCO dataset (~900 m resolution), compared to just using GEBCO alone. To explore how sensitive the results are to using different bathymetric datasets, we ran three sensitivity tests. We ran the model for a 30-day period in March 2015, using just bathymetry data from two well-known and well-used sources: (1) GEBCO [44]; and (2) ETOPO [51], which are available at resolutions of ~900 and ~775 meters, respectively. We compared the maximum current speeds and the estimated 'theoretical' power from these two runs, to a third run which used the GEBCO data merged with the higher resolution data from CICESE, for the Midriff region.

4. Results

The results are presented in three main parts: (1) analysis of currents speeds; (2) the energy resource assessment; and (3) the results of the sensitivity tests in which we ran simulations with different model mesh bathymetries.

4.1 Currents speed analysis

Hourly current vector fields over a single spring tidal cycle when the maximum velocities occur (22 March 2015) are shown in Fig. 7 for the Midriff region. Current speeds reach a maximum 3 hours after low water on the flood tide, and 3 hours after high water on the ebb tide, i.e. close to a classical standing wave. The location of Angel de la Guarda Island, to the east of the Gulf, and Tiburon Island, to the west of the Gulf, funnels the currents, first to the east of the Gulf, then to the west, on the flood tide; and vice-versa on the ebb tide.

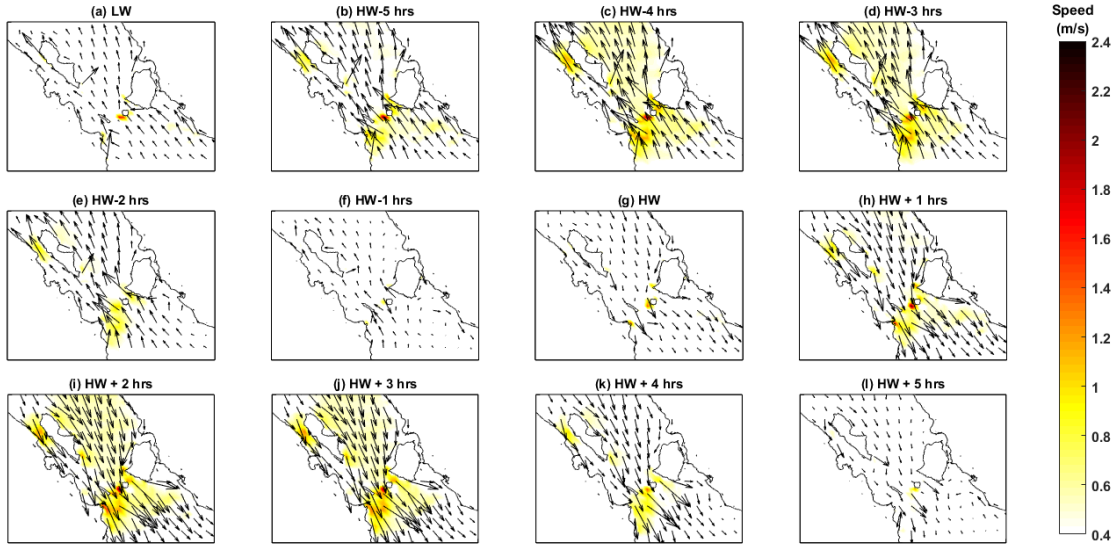

Figure 7: Velocity vectors (black arrows) and current speeds (background colour) over a single tidal cycle on the 22nd March 2015 for the Midriff region in the Gulf of California. a) Low Water b) High water - 5 hours c) High water -4 hours d) High water -3 hours e) hours e) High water – 2 hours f) High water – 1 hour g) High water h) High water + 1 hour i) High water + 2 hours j) High water + 3 hours k) High water + 4 hours l) High water + 5 hours.

The peak current speeds over the 1-month simulation are shown in Fig. 8 (note the colour scale has been altered from Fig. 7 to highlight regions with fastest currents), superimposed with bathymetry contours. Results show that maximum current speeds reach localised values of between 1 and 2.4 m/s at selected sites in the Midriff area.

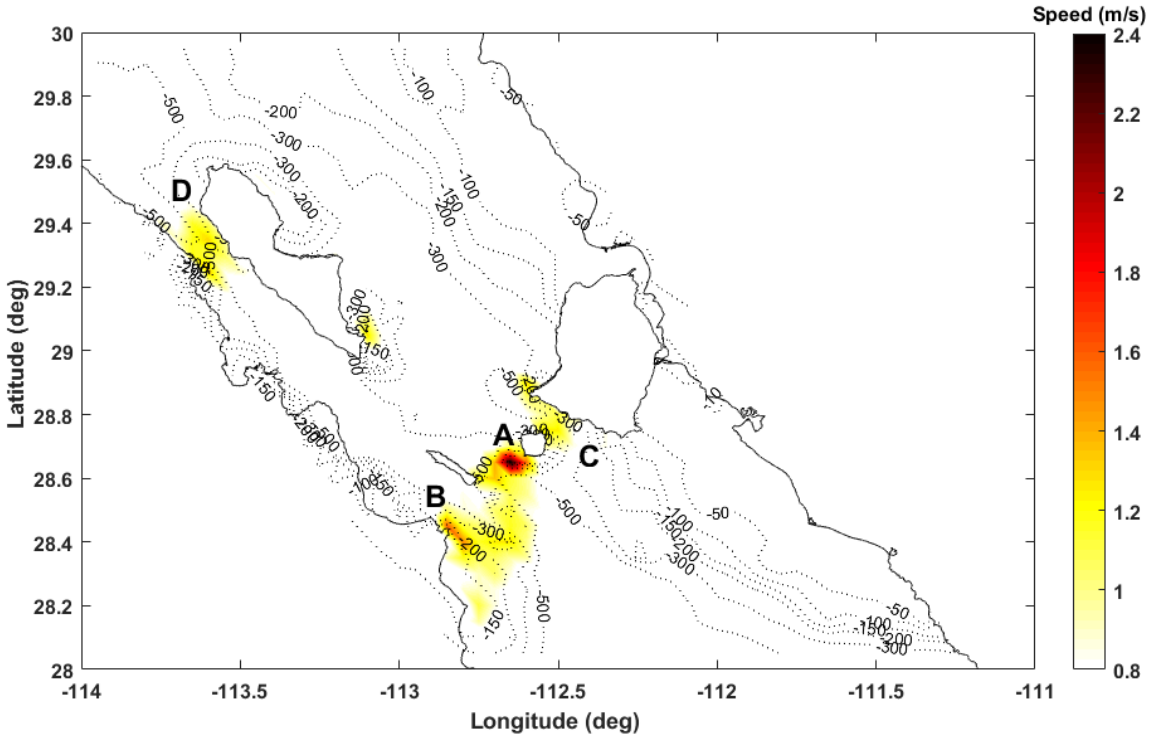

Figure 8: Maximum current speeds in the Midriff area during March 2015.

There are four main regions were current speeds exceed 1 m/s, the locations of which are marked on Fig. 8. Current speeds are largest and reach a maximum of about 2.4 m/s in the deeper-water (~500 m) channel between the San Lorenzo and San Esteban Islands (Marker A, Fig. 8). The distance between these two Islands is approximately 18 km. Current speeds of around 1.6 m/s are reached in the channel between the Baja California Peninsula and San Lorenzo Island (Marker B, Fig. 8). The fast currents occur nearer to the main land. The distance between the Baja California Peninsula and San Lorenzo Island is around 17 km. Current speeds of around 1 m/s are reached in the Channel between San Esteban and Tiburon Islands (Marker C, Fig. 8). The distance between these two Islands is 12 km. Current speeds of 1m/s also occur in the northern part of the Ballenas Channel between the Baja California Peninsula and Angel de la Guarda Island (Marker D, Fig. 8). The average width of this channel is around 14 km. Maximum current speeds at just less than 1 m/s at the south-eastern tip of Angel de la Guarda Island. Time-series of current speeds, at the grid point with fastest current speeds in each of the four main areas is shown in Fig. 9.

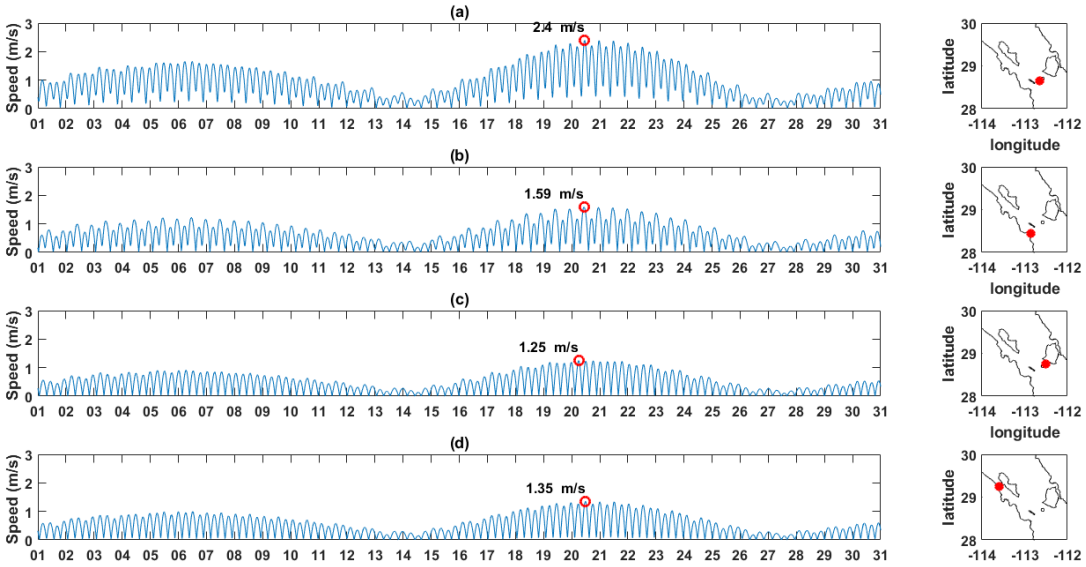

Figure 9: Time series of currents speeds in the four regions with the largest current speeds Sites location between (a) San Lorenzo (SL) and San Esteban (SE) Islands, (b) Baja California peninsula and San Lorenzo (SL) Island, (c) San Esteban (SE) and Tiburon Islands and (d) Baja California Peninsula and Angel de la Guarda Island.

The area where current speeds are in the range 1 - 1.5 m/s is 1,431 km^2. Current speeds are between 1.5 and 2 m/s in an area 70 km^2 and are greater than 2 m/s in an area 35 km^2. Sites with current speeds between 1 and 1.5 m/s are mostly situated in areas with depths greater than 100 m. Sites with velocities from 1.5 m/s and above 2 m/s are situated in depths over 120 m.

Maximum current speeds during a spring and neap period, and for the flood and ebb of a single tidal cycle, are shown in Fig. 10. Tidal current speeds are up to 1 m/s slower during a neap tide (Fig. 10b), compared to a spring tide (Fig. 10a). Currents are slightly faster during the ebb tide (Fig. 10d) compared to the flood tide (Fig. 10c).

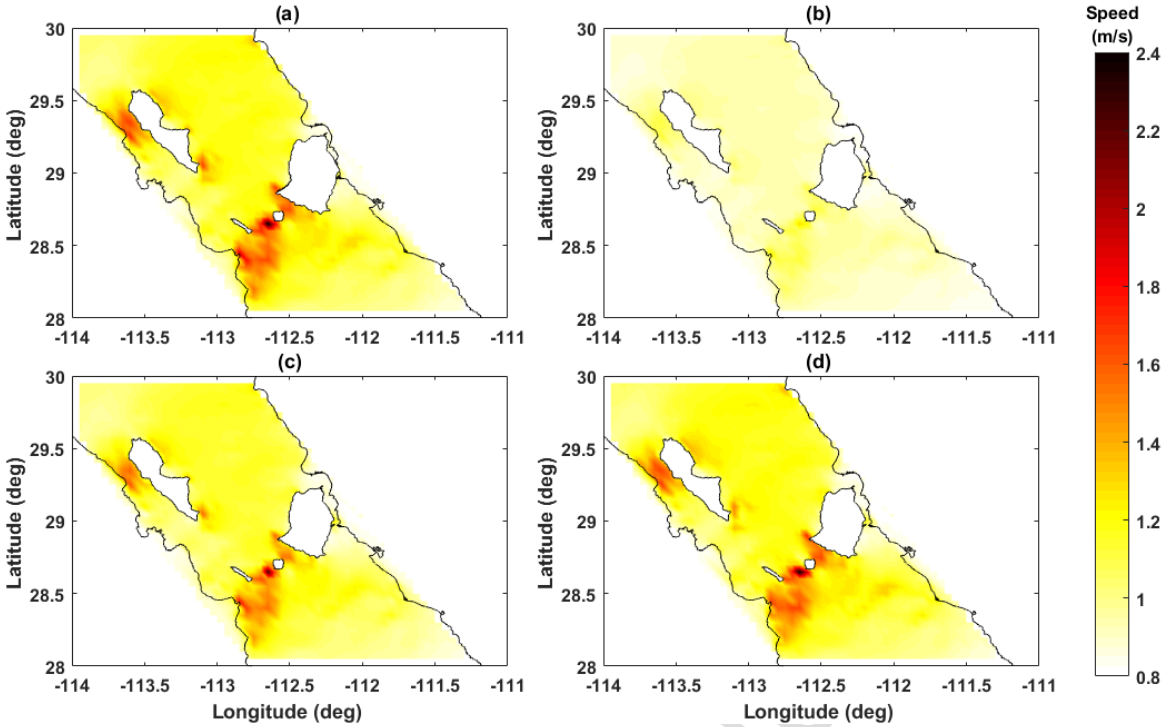

Figure 10: Maximum current speed for the (a) spring, (b) neap periods, and for the: (c) ebb and (d) flood tide, for the Midriff region in the Gulf of California.

4.2 Tidal energy resource assessment

We quantify, for the first time, the theoretical, undisturbed tidal-stream energy resource in the GC. The instantaneous theoretical KPD for the maximum currents speed (over the 1-month simulation period) is shown in Fig. 11, for the Midriff region. As expected this closely resembles the pattern of maximum current speeds, shown in Fig. 8. In the channel between the San Lorenzo and San Esteban Islands (marker A in Fig. 8), the maximum instantaneous theoretical KPD reaches 5 kW/m^2. In the other three regions, mentioned above (and shown in Fig. 8) the maximum instantaneous theoretical KPD ranges between 1.5 and 2.5 kW/m^2. Maximum instantaneous theoretical KPDs exceeds 1 kW/m^2 in an area of 384 km^2, is between 1.5 and 2.5 kW/m^2 in an area of 314 km^2 and exceeds 2.5 kW/m^2 in an area of 35 km^2.

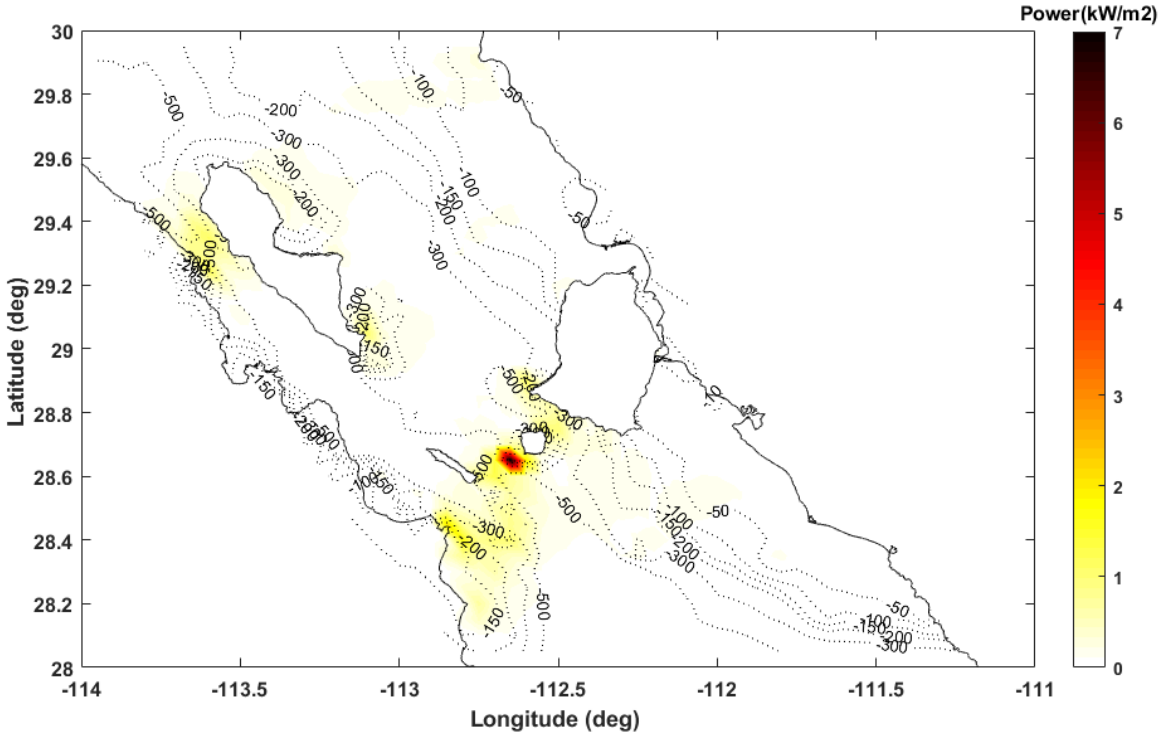

Figure 11: Maximum instantaneous undisturbed Kinetic power density, for the Midriff region in the Gulf of California.

A better measure of the available energy resource, taking into account temporal variability, is annual mean KPD (per m^2). The annual mean KPD is shown in Fig. 12a. The mean KPD range is between 0.55 and 0.65 kW/m^2 in the channel between the San Lorenzo and San Esteban Islands. In the other three regions, the annual mean power density lies between 0.1 and 0.2 kW/m^2.

We also estimated the annual maximum theoretical undisturbed mean power output, assuming, as a first order approximation, that tidal-stream turbines could utilize the full water depth and cross-sectional area of each grid cell (5 km width). The annual theoretical mean power output for the Midriff regions, is shown in Fig. 12b. The maximum annual mean power output is now in the northern part of the Ballenas Channel between the Baja California Peninsula and Angel de la Guarda Island. This is because the greater water depths in this region (~500 m), allowing for a larger overall turbine surface area, countering the slower current speeds. Here the annual theoretical mean power output exceeds 200 MW. Whilst in the other three areas the annual mean power output is between 100 and 200 MW.

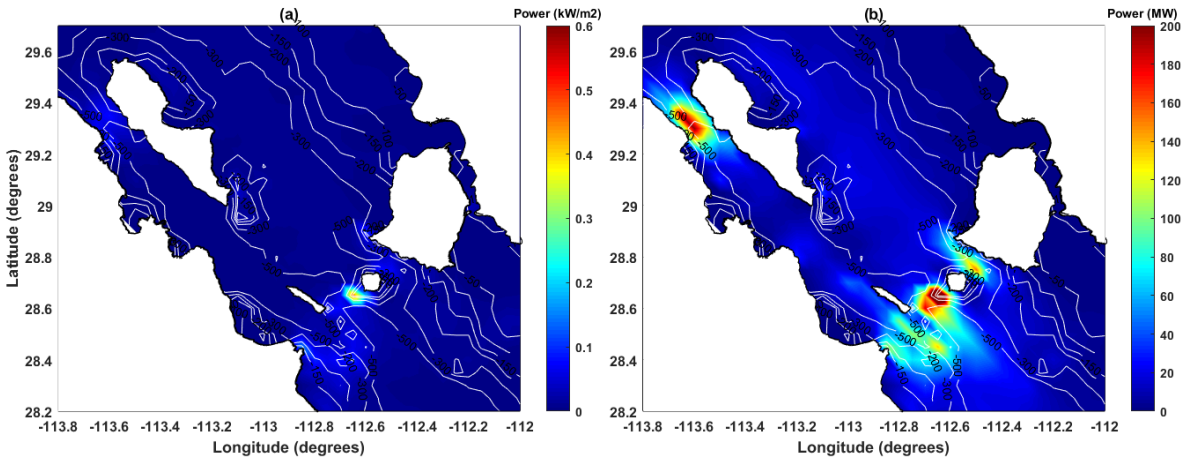

Figure 12: (a) Annual mean kinetic power density, and (b) Annual theoretical mean power, for the Midriff region in the Gulf of California. Bathymetry contours are overlaid as white lines.

4.3 Influence of bathymetry

Finally, we discuss the results of the sensitivity tests in which we estimate and compare the maximum theoretical undisturbed mean KPD and annual mean power output calculated from model runs that used: (1) just the GEBCO bathymetry; (2) just the ETOPO bathymetry; and (3) the GEBCO data merged with the higher resolution data from CICESE, for the Midriff region. The results are shown in Fig. 13. There are large differences between the runs. In regions A, B and C (shown on Fig. 8) the mean KPD and annual mean power are significantly underestimated when using along the GEBCO or ETOPO bathymetry data sources. For the region with fastest current speeds, between the San Lorenzo and San Esteban Islands (Marker A in Fig. 8), the annual mean power was around 50 MW for the GEBCO and ETOPO only runs but increased to ~200 MW for the run where the higher resolution bathymetry data from CICESE was included.

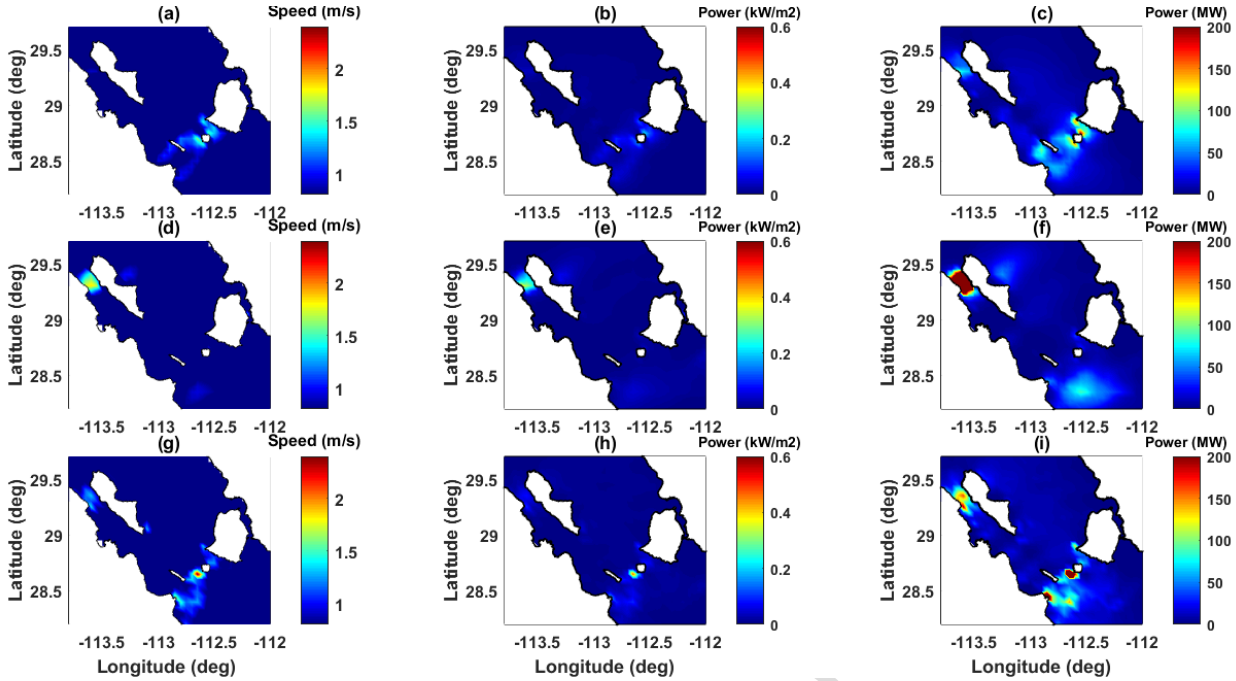

Figure 13: (b,e,h) Annual mean kinetic power density, (c,f,i) Annual mean power and (a,d,g) Maximum current speeds for (a,b,c) GEBCO only; (d,e,f) ETOPO only; and (g,h,i) GEBCO data merged with the higher resolution data from CICESE, for the Midriff region.

5. Discussion

In this paper, we have undertaken the first detailed quantification of the theoretical tidal-stream energy resource available in the GC. Although a number of parameters are significant in tidal-steam energy resource assessments, the most important is clearly current speed. In this study, peak spring velocities were found to be between 1.0 and 2.5 m/s in four main areas centred in channels in the Midriff region of the GC. The channel between San Lorenzo and San Esteban Islands shows the greatest potential for future tidal energy development, where flow speeds reach 2.4 m/s.

The maximum instantaneous KPD for the Midriff region is ~3 to 6 kW/m^2, but the mean annual KPD is much lower, ranging from 0.1 to 0.65 kW/m^2. For comparison, this represents only 10% of the maximum KPD available in the Bay of Fundy, the world's largest tidal range, and 7.5% of that predicted for Cape Spit [11]. It is currently unclear what level of annual mean KPD is needed for economic viability of tidal energy developments in the GC. This will be dependent on many factors, including (but not limited to) subsidy support, grid connection costs and technology cost reduction over time. For comparison, the 2011 UK tidal current

resource assessment conducted by Black and Veatch [52] considered sites where the mean annual KPD exceeded 1.5 kW/m^2 in depths greater than 15 m. Clearly the KPD of the GC sites fall below this 1.5 kW/m^2 threshold. However, although the average KPD, and corresponding current speeds, are lower than recommendations for economic feasibility [52], the greater water depths (as discussed above), account for an overall greater power potential than for several sites in shallower water and with higher velocities. Depths at the GC sites far exceed that of 15 m and were found to occur in water depths of over 100 m, removing the constraint set by depth on allowable turbine swept area per turbine. As a comparison with other potential tidal-stream energy sites around the world, the deepest sites evaluated in these other studies are typically less than 80 m, and mostly less than 50 m.

Therefore, the analysis of the distribution of the undisturbed KPD suggests that the four sites identified in this initial resource assessment of the GC are unsuitable for 1st generation tidal stream turbine technology. However, with investment and development in appropriate technology suitable for deeper water locations, sites within the GC could become feasible development opportunities in the future. This would also allow other similar sites to be utilized to increase the practical available resource worldwide. As occurred with wind energy [1], new global markets should promote investment in tidal-stream energy extraction research [53]. Prototypes, trials and knowledge of deep and low flow extraction devices will actively help to close the deep flow energy extraction knowledge gap. New technologies capable of operating at these deeper depths, and new energy policies can help reduce the current costs of marine energy extraction to open up opportunities at deeper, lower flow sites. It is also acknowledged in Black & Veatch [52] that 'technologies specifically designed for low power density sites (such as the Minesto device) could potentially result in lower power density sites becoming economic'.

We stress that we have estimated only the theoretical, undisturbed tidal-stream energy resource for the GC. To further this study, effects such as array scale blockage [54], array-array interaction [13], wake-turbine interaction [55] and array optimisation [56] also need to be considered. This relies on implementing additional drag terms in the momentum equations to simulate turbine drag. Select past numerical modelling studies have included the effect of turbine drag [e.g. 57, 58, 59, 60, and 61]. Therefore, one important consideration, for future work, would be to determine flow reduction across the GC as a result of tidal stream energy extraction, and consideration for optimal array layout. Nevertheless, our simple approach has

allowed us to provide a first estimate of the annual mean and maximum theoretical tidal-stream energy resource to inform the industry and policy, upon which more detailed further studies can be built.

Our results show that there are significant temporal variations in current speeds, and hence, the energy resource, over single tidal cycles (i.e. tidal asymmetry) and longer periods. These are due to the fact that tides in the Midriff region are mixed in form, as a result of relatively large semi-diurnal and diurnal tidal constituents. These factors, particularly the tidal asymmetry, need to be taken into account when planning for future device installations [62]. In addition, we have shown that correctly predicting tidal currents requires accurate, high resolution bathymetric data. We therefore caution the used of applying global bathymetric data products for tidal-energy resource assessment in regions where relatively little 'freely available' data is accessible.

Due to the complexity of setting up a full three-dimensional baroclinic model, and the associated longer model run times, we decided to base our initial resource assessment, presented here, on a depth-averaged tidal model. The potential tidal-stream energy sites we identified are in water depths >100 m, where three-dimensional flows will clearly be important. Previous oceanographic studies [e.g. 38,39] have shown that the GC is subject to strong seasonal stratification, which will influence the vertical structure of tidal currents. In the future, we hope to configure and run a full three-dimensional model, to examine the vertical structure of tidal currents in the area of interest. The drag coefficient methodology developed by Blunden and Bahaj [5] could be applied to simulate the presence of a turbine array. In past studies the drag coefficient has been applied at the seabed, as suitable sites are in shallow water. However, a momentum sink could be applied to different vertical layers through the water column.

Grid connectivity in the region presents a challenge. The nearest electricity connection point for the three southern sites we have identified is located more than 35 km away at Kino Bay, requiring any cabling to cross the complex mountains on Tiburon Island. For the northern site, in the Ballenas channel, the closest connectivity point is that of Bahia de Los Angeles, more than 40 km south-west. Furthermore, the difficult access to the region due to its topography, dry weather, and lack of fresh water make this area unattractive for urban development. Therefore, the tidal-stream energy that could be converted into electricity from the GC might be more suitable for off-grid applications.

6. Conclusions

The aim of this paper was to undertake the first tidal-stream energy resource assessment for the Gulf of California in México. In contrast to other regions in which the tidal stream energy resource has been explored, the GC is relatively deep, and diurnal tidal constituents are typically larger. Hence the resource characterization was expected to contrast considerably from previously identified tidal stream sites. As part of this study, a depth-averaged barotropic hydrodynamic model was configured using the TELEMAC suite of modelling tools and the model was validated against tide gauge and current records, demonstrating good accuracy.

Model predictions show peak current speeds of up to 2.4 m/s in the Midriff area and its straits. We found that there are four main locations where the tidal current speeds exceeded 1.0 m/s: (1) in channel between the San Lorenzo and San Esteban Islands – here maximum current speeds are close to 2.4 m/s; (2) in the channel between the Baja California Peninsula and San Lorenzo Island; (3) in the Channel between San Esteban and Tiburon Island; and (4) in the northern part of the Ballenas Channel between the Baja California Peninsula and Angel de la Guarda Island.

The maximum instantaneous undisturbed 'theoretical' kinetic power density in the Midriff region was estimated to be between 3 and 6 kW/m^2, but the mean annual KPD is much lower, ranging from 0.1 to 0.65 kW/m^2. However, as the sites with tidal current speeds typically exceed 100 m in water depth, we estimate the maximum undisturbed theoretical annual mean power to be 100 to 200 MW. We therefore find the tidal energy resource to be large, but new turbine technologies would be required to exploit these 'second generation' resource regions. Moreover, whereas our simulations are based on localised refined bathymetry datasets, global and freely available bathymetry data products under-resolve the resource by 75%.

This assessment has provided an overall first order estimate of the available tidal-stream energy resource in the Gulf. It will provide a basis for more detailed analyses to guide selection of suitable sites for tidal–stream energy extraction in the region.

Acknowledgements

We thank Dr. Silvio Guido Marinone from CICESE research centre for providing the higher resolution bathymetry data for the Gulf of California and Dr. Antonio Hernandez for the ADCP dataset. This research was partially financed by CONACyT (the National Council of Science and Technology) through the grant "Becas en el extranjero 2014-1" grant reference CVU 536867 and also the research was funded by the University of Southampton. Matt Lewis and Simon Neill were supported by the NRN-LCEE QUOTIENT project", funded by the Welsh Government and the Higher Education Funding Council for Wales (HEFCW), through the National Research Network for Low Carbon, Energy, and the Environment (NRN-LCEE).

References

[1] Bahaj, A. & Myers, L., (2004). Analytical Estimates of Energy Yield Potential from the Alderney Race (Channel Islands) using Marine Current Energy Converters. Renewable Energy, 29, pp.1931-45.

[2] OES (2012), An international Vision for energy, Ocean energy systems implementation agreement, 5th GMREC Annual Conference 24 - 26 April 2012.

[3] Fraenkel, P., (2006). Tidal Marine current turbines: Pioneering the development of marine kinetic energy converters. Proceedings of the Institution of Mechanical Engineers Part A Journal of Power and Energy (P I MECH ENG A-J POW).

[4] Garrett, C., & P. Cummins (2008). Limits to tidal current power. Renewable Energy, 33, pp. 2485-2490.

[5] Blunden, L. & Bahaj, A., (2006). Initial Evolution of Tidal Stream Energy Resources at Portland Bill, UK. Renewable Energy, 31, pp.121-32.

[6] Adcock, T. A. A., Draper, S., Houlsby, G. T., Borthwick, A. G. L. & Serhadlioglu, S. (2013). The available power from tidal stream turbines in the Pentland Firth. Proceedings of the Royal Society A: Mathematical, Physical and Engineering Science, 469.

[7] Serhadlıoğluet, S., Adcock, T. A. A., Houlsby, G. T., Draper, S. & Borthwick, A. G. L. 2013. Tidal stream energy resource assessment of the Anglesey Skerries. International Journal of Marine Energy, 3–4, e98-e111.

[8] Lewis, M., Neill, S. P., Robins, P. E. & Hashemi, M. R. (2015). Resource assessment for future generations of tidal-stream energy arrays. Energy, 83, 403-415.

[9] Sutherland, G., Foreman, M. & Garrett, C. (2007). Tidal current energy assessment for Johnstone Strait, Vancouver Island. Proceedings of the Institution of Mechanical Engineers, Part A: Journal of Power and Energy, 221, 147-157.

[10] Karsten, R.H., J.M. McMillan, M.J. Lickley, and R.D. Haynes (2008). Assessment of tidal current energy in the Minas Passage, Bay of Fundy. Proceedings of the Institution of Mechanical Engineers Part A: Journal of Power and Energy, 222, pp. 493-507.

[11] Cornett A, Noemie Durand, Martin Serrer (2010). 3-D Modelling and Assessment of Tidal Current Resources in the Bay of Fundy, Canada 3rd International Conference on Ocean Energy, 6 October, Bilbao

[12] Myers, L. & Bahaj, A., (2005). Simulated Electrical Power Potential Harnessed by Marine Current Turbine Arrays in the Alderney Race. Renewable Energy, 30, pp.1713-31.

[13] Coles, D. S., Blunden, L. S. & Bahaj, A. S. 2017. Assessment of the energy extraction potential at tidal sites around the Channel Islands. Energy, 124, 171-186.

[14] Guillou, N., Neill, S. P. & Robins, P. E. (2018). Characterising the tidal stream power resource around France using a high-resolution harmonic database. Renewable Energy, 123, 706-718.

[15] Grabbe, M., E. Lalander, S. Lundin and M. Leijon (2009). "A review of the tidal current energy resource in Norway." Renewable and Sustainable Energy Reviews 13(8): 1898-1909.

[16] Calero Quesada, M. C., García Lafuente, J., Sánchez Garrido, J. C., Sammartino, S. & Delgado, J. (2014). Energy of marine currents in the Strait of Gibraltar and its potential as a renewable energy resource. Renewable and Sustainable Energy Reviews, 34, 98-109.

[17] Gonzalez-Caballín, J. M., Álvarez, E., Guttiérrez-Trashorras, A. J., Navarro-Manso, A., Fernández, J. & Blanco, E. (2016). Tidal current energy potential assessment by a two dimensional computational fluid dynamics model: The case of Avilés port (Spain). Energy Conversion and Management, 119, 239-245.

[18] Blunden, L. S., Bahaj, A. S. & Aziz, N. S. (2013). Tidal current power for Indonesia? An initial resource estimation for the Alas Strait. Renewable Energy, 49, 137-142."Tidal current power for Indonesia? An initial resource estimation for the Alas Strait." Renewable Energy 49: 137-142.

[19] Orhan, K., Mayerle, R. & Pandoe, W. W. (2015). Assessment of Energy Production Potential from Tidal Stream Currents in Indonesia. Energy Procedia, 76, 7-16.

[20] Chen, W.-B., Liu, W.-C. & Hsu, M.-H. (2013). Modelling assessment of tidal current energy at Kinmen Island, Taiwan. Renewable Energy, 50, 1073-1082.

[21] Gao, P., Zheng, J., Zhang, J. & Zhang, T. (2015). Potential Assessment of Tidal Stream Energy around Hulu Island, China. Procedia Engineering, 116, 871-879.

[22] Lim, Y. S. and S. L. Koh (2010). "Analytical assessments on the potential of harnessing tidal currents for electricity generation in Malaysia." Renewable Energy 35(5): 1024-1032.

[23] Buhali, M. L., Abundo, M. L. S. & ANG, M. R. C. O. Site selection procedures for tidal in-stream energy in the Philippines: A Preliminary Study. 2012 10th International Power & Energy Conference (IPEC), 12-14 Dec. 2012 2012. 110-114.

[24] Plew, D. R. and C. L. Stevens (2013). "Numerical modelling of the effect of turbines on currents in a tidal channel – Tory Channel, New Zealand." Renewable Energy 57: 269-282.

[25] Moore, T. & Boyle, C. 2014. The tidal energy potential of the Manukau Harbour, New Zealand. Sustainable Energy Technologies and Assessments, 8, 66-73.

[26] Alemán-Nava, G. S., Casiano-Flores, V. H., Cárdenas-Chávez, D. L., Díaz-Chavez, R., Scarlat, N., Mahlknecht, J., Dallemand, J.-F. & Parra, R. (2014). Renewable energy research progress in Mexico: A review. Renewable and Sustainable Energy Reviews, 32, 140-153.

[27] Osorio, A. F., Ortega, S. & Arango-Aramburo, S. (2016). Assessment of the marine power potential in Colombia. Renewable and Sustainable Energy Reviews, 53, 966-977.

[28] Herrera, R., Vásquez, J., Cienfuegos, R., Olivares, M. (2010). Análisis de Factibilidad Técnico-Económico del Recurso Energético Asociado a las Corrientes de Marea en el Canal del Chacao. Available at http://www.repositorio.uchile.cl/handle/2250/103697.

[29] González-Gorbeña, E., Rosman, P. C. C. & Qassim, R. Y. 2015. Assessment of the tidal current energy resource in São Marcos Bay, Brazil. Journal of Ocean Engineering and Marine Energy, 1, 421-433.

[30] Marta-Almeida, M., Cirano, M., Guedes Soares, C. & Lessa, G. C. 2017. A numerical tidal stream energy assessment study for Baía de Todos os Santos, Brazil. Renewable Energy, 107, 271-287.

[31] Alonso, R., Jackson, M., Santoro, P., Fossati, M., Solaris, S. & Teixeira, L. 2017. Wave and tidal energy resource assessment in Uruguayan shelf seas. Renewable Energy.

[32] SENER, Secretaria de Energia (2013), Estrategia Nacional 2013-2027, Available at http://www.sener.gob.mx/res/PE_y_DT/pub/2013/ENE_2013-2027.pdf [Accessed 10 December 2014]

[33] NRDC (2017) Mexico ratifies the Paris agreement. [Online]. Available from https://www.nrdc.org/experts/amanda-maxwell/mexico-ratifies-paris-agreement [Accessed March 2017].

[34] Hiriart-Le Bert G. and Silva-Casarin R., (2009). Tidal Power plan energy estimation. Engineering Institute, Autonomous National University of Mexico. Mexico. 11 (2) 233-245,

[35] Tapia Olivas, J. C., Ramírez Campbell, H. E. & Gil Samaniego Ramos, M. 2013. Feasibility Analysis for a Tidal Energy Pilot Site in the Gulf of California. V06BT07A087.

[36] Badan-Dangon, A., M. C. Hendershott, and M. F. Lavın (1991), Underway Doppler current profiles in the Gulf of California, Eos Trans. AGU, 72(209), 217 – 218.

[37] Lopez, M., Candela, J. & Garcia, J. (2008). Two overflows in the Northern Gulf of California. Journal of Geophysical Research: Oceans, 113, n/a-n/a.

[38] Lavın M. F. and S. Organista. (1988), Surface heat flux in the northern Gulf of California. J. Geophysics. Res., 93, 14033-14038.

[39] Alvarez-Borrego, S., and J.R. Lara-Lara (1991). The physical environment and primary productivity of the Gulf of California. In The Gulf and Peninsular Province of the Californias, Mem. Am. Assoc. Pet. Geol., 47, 555-567.

[40] Filloux, J.H.(1973). Tidal patterns and energy balance in the Gulf of California. Nature, 217-221,

[41] Ripa, P. and G. Velazquez (1993). Modelo unidimensional de la marea en el Golfo de California. Geofis. Intl., 32, 41-56.

[42] Marinone, S.G. (2000) Tidal Currents in the Gulf of California: Intercomparison among two and three-dimensional models with observations. Cienc. Mar., 26, 275-301.

[43] Jean-Michel Hervouet, "Hydrodynamics of Free Surface Flows: Modelling with the Finite Element Method", Wiley Blackwell, April 2007, 360p, ISBN-13: 978-0470035580.

[44] Kapoor, D.C., (1981). General bathymetric chart of the oceans (GEBCO). Marine Geodesy, 5(1), pp.73–80.

[45] Egbert, G. D., A. F. Bennet, and M. G. G. Foreman (1994), Topex/Poseidon tides estimated using a global inverse model, Journal of Geophysical Research, 99, 24,821 24,852.

[46] Egbert, G. D. and S. Y. Erofeeva (2002). "Efficient Inverse Modeling of Barotropic Ocean Tides." Journal of Atmospheric and Oceanic Technology 19(2): 183-204.

[47] Haigh, I. D., M. Eliot, and C. Pattiaratchi (2011b). "Global influences of the 18.61 year nodal cycle and 8.85 year cycle of lunar perigee on high tidal levels." Journal of Geophysical Research: Oceans 116(C6).

[48] Laboratorio de nivel del mar Cicese [online] Estaciones Mareográficas y Meteorológicas Costeras. Available from: http://redmar.cicese.mx/.[Accessed July 2016].

[49] Pawlowicz R, Beardsley B, Lentz S (2002). Classical tidal harmonic analysis including werror estimates in MATLAB using T_TIDE. Comput Geosci. 28(8):929–37.

[50] Myers, L. & Bahaj, A. (2005), Simulated Electrical Power Potential Harnessed by Marine Current Turbine Arrays in the Alderney Race. Renewable Energy, 30, pp.1713-31.

[51] NOAA (2017). ETOPO1 Global Relief Model [online] United States of America. Available from https://www.ngdc.noaa.gov/mgg/global/. [Accessed March 2017].

[52] Black & Veatch, (2005b). Phase II UK Tidal Stream Energy Resource Assessment. London: The Carbon Trust.

[53] Bahaj A. S. (2013). Marine current energy conversion: the dawn of a new era in electricity production. Philosophical Transactions of the Royal Society A: Mathematical, Physical and Engineering Sciences, 371.

[54] Garrett, C., & P. Cummins (2008). Limits to tidal current power. Renewable Energy, 33, pp. 2485-2490.

[55] Abolghasemi, M. A., Piggott, M. D., Spinneken, J., Virí, A., Cotter, C. J. & Crammond, S. 2016. Simulating tidal turbines with multi-scale mesh optimisation techniques. Journal of Fluids and Structures, 66, 69-90.

[56] Funke, S. W., Kramer, S. C. & Piggott, M. D. 2016. Design optimisation and resource assessment for tidal-stream renewable energy farms using a new continuous turbine approach. Renewable Energy, 99, 1046-1061.

[57] Neill, S. P., Litt, E. J., Couch, S. J. & Davies, A. G. (2009). The impact of tidal stream turbines on large-scale sediment dynamics. Renewable Energy, 34, 2803-2812.

[58] Ahmadian, R., Falconer, R. & Bockelmann-Evans, B. (2012), Far-field modelling of the hydro-environmental impact of tidal stream turbines. Renewable Energy, 38, 107-116.

[59] Neill, S. P., Jordan, J. R. & Couch, S. J. (2012), Impact of tidal energy converter (TEC) arrays on the dynamics of headland sand banks. Renewable Energy, 37, 387-397.

[60] O'Donncha, F., Hartnett, M. & Nash, S. (2013), Physical and numerical investigation of the hydrodynamic implications of aquaculture farms. Aquacultural Engineering, 52, 14-26.

[61] Goward Brown, A., Neill, S.P., Lewis, M.J. (2017) Tidal energy extraction in three-dimensional ocean models. Renewable Energy (in press).

[62] Neill, S.P., Hashemi, M.R. and Lewis, M.J. (2014) The role of tidal asymmetry in characterizing the tidal energy resource of Orkney. Renewable Energy 68, 337-350.

Gulf of California (Mexico) simulated with a barotropic model

Predicted peak tidal flows between 1.0 and 2.4 m/s at sites in the Gulf of California

Theoretical tidal-stream power density estimates at four sites were ~ 3 to 6 kW/m^2

Potential tidal stream sites in deep water (100 to 500 m)

New technologies would be required to exploit these non-traditional regions